V European Conference on Computational Fluid Dynamics
ECCOMAS CFD 2010
J. C. F. Pereira and A. Sequeira (Eds)
Lisbon, Portugal,14-17 June 2010

COHERENT VORTICITY AND CURRENT EXTRACTION IN THREE-DIMENSIONAL HOMOGENEOUS MAGNETOHYDRODYNAMIC TURBULENCE: COMPARISON BETWEEN WAVELET AND FOURIER FILTERING

Naoya Okamoto*, Katsunori Yoshimatsu†, Yuji Kondo†, Kai Schneider†† and Marie Farge†††

*Center for Computational Science, Nagoya University,
Furo-cho, Chikusa-ku, Nagoya, 464-8603, Japan
e-mail: okamoto@ccs.engg.nagoya-u.ac.jp
†Department of Computational Science Engineering, Nagoya University
Furo-cho, Chikusa-ku, Nagoya, 464-8603, Japan
e-mail: {yosimatu, kondo}@fluid.cse.nagoya-u.ac.jp
††M2P2-CNRS and CMI, Université de Provence
39 rue Frédéric Joliot-Curie, 13453 Marseille Cedex 13, France
e-mail: kschneid@cmi.univ-mrs.fr
†††LMD-IPSL-CNRS, Ecole Normale Supérieure
24 rue Lhomond, 75231 Paris Cedex 05, France
e-mail: farge@lmd.ens.fr

Key words: wavelet methods, turbulence modeling, numerical magnetohydrodynamics, homogeneous turbulence, coherent structure

Abstract. *A method for extracting coherent vorticity sheets and current sheets out of three-dimensional homogeneous magnetohydrodynamic (MHD) turbulence, called the CVCE method, is proposed and compared with linear Fourier filtering (LFF) method. The CVCE method is based on the orthogonal wavelet decomposition of the vorticity and current density fields. Thresholding the wavelet coefficients allows both fields to be split into coherent and incoherent parts. The LFF method is based on the Fourier decomposition, which decomposes a given field into large- and small-scale contributions. These methods are applied to direct numerical simulation (DNS) data of three-dimensional homogeneous MHD turbulence in a periodic box. It is found that the coherent structures extracted by using the CVCE method, represented by a few percent of the number of degrees of freedom of the DNS field, well preserve the vorticity sheets and current density sheets present in the DNS field. The incoherent vorticity and current density are shown to be structureless. On the other hand, the large-scale fields obtained by the LFF method, represented by almost the same number of degrees of freedom as that for the coherent fields, do not well preserve the vorticity sheets and current density sheets present in the DNS field. The small-scale vorticity and current density fields contain organized structures similar to those present in the DNS field. We examine the contributions of these coherent, incoherent, large-scale and small-scale fields and compare their statistics with the DNS field.*

1 INTRODUCTION

Understanding the role of coherent structures in turbulence is a prerequisite for accurate and physically-based modeling of turbulence. The structures are not distributed homogeneously and turbulent fields exhibit spatial intermittency. This means that the spatial support of coherent structures decreases with scale, as a result, the nonlinear activity becomes localized at small scale. To be able to benefit from this property, a suitable representation of such intermittent fields should take into account this lacunarity.

The wavelet transform decomposes a given field into scale-space contributions, which allows for a sparse representation of intermittent data. For the intermittent data, the small scale contributions have significant values only in active regions and are nonsignificant in weak regions. If the nonsignificant contributions are negligible in the dynamics of turbulence, the amount of wavelet coefficients can thus be significantly reduced before reconstructing the flow field in physical space. For a review on applications of wavelet methods to turbulence we refer to Refs. 1 and 2.

The coherent vorticity extraction (CVE) method introduced for two- and three-dimensional hydrodynamic (HD) turbulence[3,4,5] is one of the most useful tools for the extraction of coherent vortices from HD turbulence together with a significant reduction of the number of degrees of freedom. It is based on orthonormal wavelets which yield a non-redundant representation and for which fast transformation algorithms are available[6]. The CVE method allows us to divide the vorticity field into two orthogonal parts, coherent and incoherent vorticity. The coherent vorticity reconstructed from few wavelet coefficients of vorticity, whose moduli are above a threshold, which is motivated from denoising theory[7], contains the coherent vortex tubes, and exhibits statistics similar to those of the total vorticity. The incoherent vorticity reconstructed from the remaining large majority of the wavelet coefficients corresponds to an almost uncorrelated random background. The CVE method was applied to direct numerical simulation (DNS) data of three-dimensional homogeneous isotropic turbulence in a periodic box[4,5,8]. Only about 3% of the wavelet coefficients of vorticity represent the coherent vortex tubes, and they well preserve statistics of the DNS data. Farge *et al.* compared the CVE method with linear Fourier filtering (LFF) one, using the spectral cutoff filter[4]. The CVE method is shown to be more efficient than the LFF method for extracting the coherent vortex tubes out of the turbulent flow. The CVE method has great potential for application to other types of intermittent fields, since it is based only on the flow intermittency.

Recently, the CVE method has been generalized to extract coherent vorticity sheets and coherent current sheets out of three-dimensional homogeneous magnetohydrodynamic (MHD) turbulence[9]. We call the method Coherent Vorticity sheet and Current sheet Extraction (CVCE) method. The method was applied to DNS data of incompressible MHD turbulence without mean magnetic field in a 2π periodic box. The coherent vorticity and current density fields preserve both the vorticity sheets and the current sheets present in the DNS field, while retaining only a few percent of the number of degrees of freedom.

The incoherent vorticity and current density are shown to be structureless and of mainly dissipative nature.

In the present study, we summarize the statistics of the coherent and incoherent fields obtained by the CVCE method, and compare the CVCE method with the LFF method.

2 EXTRACTION OF COHERENT STRUCTURE

In this section, we briefly summarize the CVCE method[9], and describe the LFF method.

2.1 CVCE method

A wavelet-based nonlinear filtering method for extracting coherent vorticity and coherent current density from three-dimensional homogeneous MHD turbulent field, called the CVCE method, was proposed[9]. The coherent vorticity and coherent current density are defined by '*what remains after denoising*'.

Both fields, vorticity $\boldsymbol{\omega}$ and current density $\boldsymbol{j}$, are first decomposed into orthogonal wavelet series. Then we split each field into coherent and incoherent contributions in wavelet space by applying nonlinear thresholding. The coherent vorticity field $\boldsymbol{\omega}_\mathrm{c}$ is reconstructed from the wavelet coefficients whose moduli are larger than a given threshold. The coherent current density field $\boldsymbol{j}_\mathrm{c}$ is obtained in the same way as in the case of $\boldsymbol{\omega}_\mathrm{c}$. The threshold value for the current density field can be different from that for the vorticity field. The incoherent fields are obtained by means of simple subtraction, $\boldsymbol{\omega}_\mathrm{i} = \boldsymbol{\omega} - \boldsymbol{\omega}_\mathrm{c}$ and $\boldsymbol{j}_\mathrm{i} = \boldsymbol{j} - \boldsymbol{j}_\mathrm{c}$. The coherent and incoherent contributions for each field thus obtained are orthogonal, which ensures a separation of the total kinetic and magnetic enstrophies, defined as $Z^u = \langle \boldsymbol{\omega}, \boldsymbol{\omega} \rangle / 2$ and $Z^b = \langle \boldsymbol{j}, \boldsymbol{j} \rangle / 2$, into $Z^u = Z^u_\mathrm{c} + Z^u_\mathrm{i}$ and $Z^b = Z^b_\mathrm{c} + Z^b_\mathrm{i}$, respectively. Here, $Z^u_\mathrm{c} = \langle \boldsymbol{\omega}_\mathrm{c}, \boldsymbol{\omega}_\mathrm{c} \rangle / 2$, $Z^u_\mathrm{i} = \langle \boldsymbol{\omega}_\mathrm{i}, \boldsymbol{\omega}_\mathrm{i} \rangle / 2$, $Z^b_\mathrm{c} = \langle \boldsymbol{j}_\mathrm{c}, \boldsymbol{j}_\mathrm{c} \rangle / 2$, and $Z^b_\mathrm{i} = \langle \boldsymbol{j}_\mathrm{i}, \boldsymbol{j}_\mathrm{i} \rangle / 2$. Hereafter, the superscript u stands for the velocity field and b for the magnetic field, corresponding to the vorticity and current density fields, respectively.

Biot-Savart's relations, $\boldsymbol{u}_\alpha = -\nabla \times (\nabla^{-2} \boldsymbol{\omega}_\alpha)$ and $\boldsymbol{b}_\alpha = -\nabla \times (\nabla^{-2} \boldsymbol{j}_\alpha)$, $(\alpha = \mathrm{c}, \mathrm{i})$, are used to reconstruct the coherent velocity field $\boldsymbol{u}_\mathrm{c}$, the incoherent velocity field $\boldsymbol{u}_\mathrm{i}$, the coherent magnetic field $\boldsymbol{b}_\mathrm{c}$ and the incoherent magnetic field $\boldsymbol{b}_\mathrm{i}$ from $\boldsymbol{\omega}_\mathrm{c}$, $\boldsymbol{\omega}_\mathrm{i}$, $\boldsymbol{u}_\mathrm{c}$ and $\boldsymbol{u}_\mathrm{i}$, respectively.

2.2 LFF method

In the LFF method, vorticity $\boldsymbol{\omega}$ and current density $\boldsymbol{j}$ are decomposed into Fourier series. The large-scale vorticity $\boldsymbol{\omega}_\mathrm{L}$ and the large-scale current density $\boldsymbol{j}_\mathrm{L}$ are obtained by retaining only the Fourier coefficients whose wavenumbers $k = |\boldsymbol{k}|$ are smaller than the cutoff wavenumber, i.e. $k < k_\mathrm{c}$, where $\boldsymbol{k}$ is the wave vector. The remaining small-scale vorticity $\boldsymbol{\omega}_\mathrm{S}$ and small-scale current density $\boldsymbol{j}_\mathrm{S}$ are reconstructed from the Fourier coefficients satisfying $k \geq k_\mathrm{c}$, and are also simply obtained by $\boldsymbol{\omega}_\mathrm{S} = \boldsymbol{\omega} - \boldsymbol{\omega}_\mathrm{L}$ and $\boldsymbol{j}_\mathrm{S} = \boldsymbol{j} - \boldsymbol{j}_\mathrm{L}$. Here, we determine the cutoff wavenumber k_c so that the percentage of the number of the

Fourier coefficients whose wavenumbers are smaller than k_c is almost the same as that of the wavelet coefficients representing the coherent fields extracted by the CVCE method.

3 NUMERICAL RESULTS

We first summarize the statistics of coherent and incoherent fields which were obtained by the use of the CVCE method[9]. They are compared with the statistics of large- and small-scale fields obtained by the LFF method. Both methods are applied to the DNS data of incompressible MHD turbulence in a 2π periodic box, computed at resolution $N = 512^3$. The Taylor microscale Reynolds number of MHD turbulence and the Prandtl number are 154 and 1, respectively[9].

3.1 Results obtained by CVCE method

3.1.1 Visualization

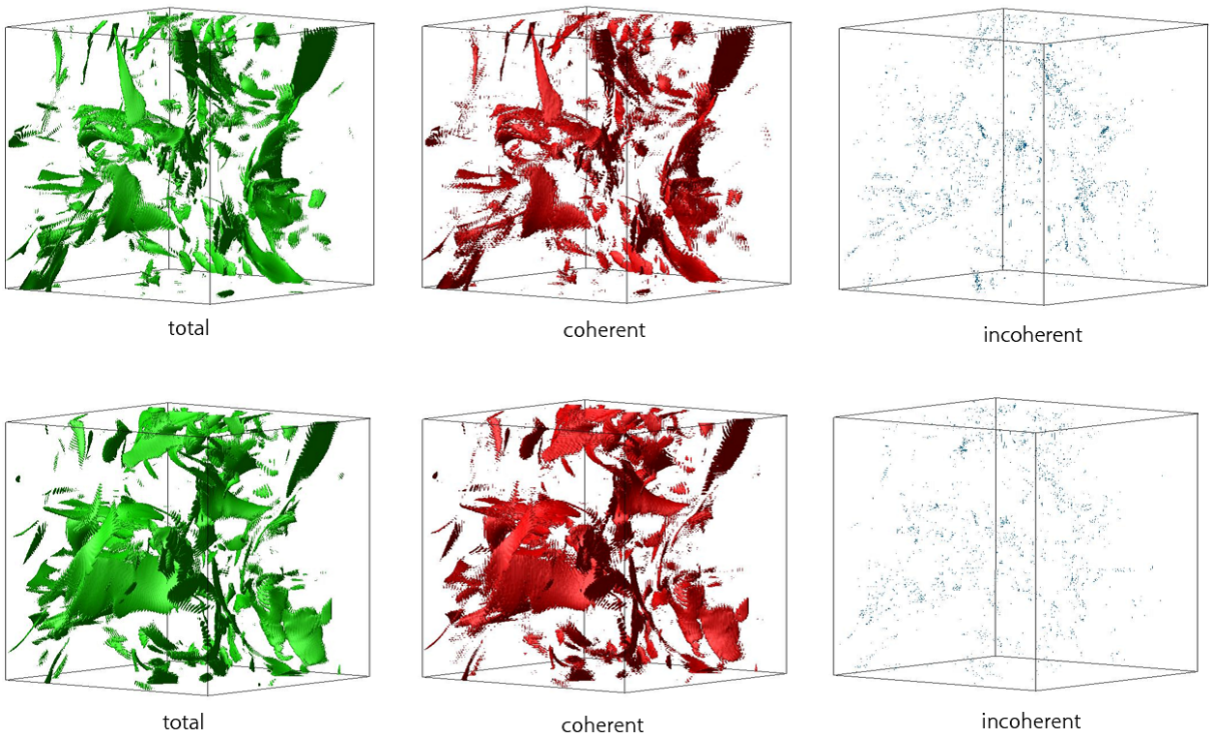

Figure 1: Isosurfaces of vorticity $|\boldsymbol{\omega}|$ (top) and current density $|\boldsymbol{j}|$ (bottom) of the total (left), coherent (middle), and incoherent contributions (right). The values of the isosurfaces are taken as $|\boldsymbol{\omega}| = \langle\omega_t\rangle + 4\sigma_\omega$ for the total and coherent vorticity and $|\boldsymbol{j}| = \langle j_t\rangle + 4\sigma_j$ for the current density. For the incoherent vorticity and current density fields, the isosurfaces are set to $|\boldsymbol{\omega}| = (\langle\omega_t\rangle + 4\sigma_\omega)/3$ and $|\boldsymbol{j}| = (\langle j_t\rangle + 4\sigma_j)/3$, respectively. Here, $\langle\omega_t\rangle$ and $\langle j_t\rangle$ are the mean values of $|\boldsymbol{\omega}|$ and $|\boldsymbol{j}|$ for the total vorticity and current density fields, respectively, and σ_ω and σ_j are standard deviation values of $|\boldsymbol{\omega}|$ and $|\boldsymbol{j}|$, respectively. Subcubes of size 256^3 are visualized.

Figure 1 (left) shows isosurfaces of intense vorticity (top) and current density (bottom) regions of the total fields (green) in the DNS data. We see vorticity and current density sheets as in previous DNS results (e.g., Refs. 10 and 11). Note that the threshold value used in the visualization for the vorticity field is different from that for the current density field. We show isosurfaces of the coherent vorticity and current density (red) in Fig. 1 (middle). The coherent vorticity and current density fields, plotted with the same isosurface values as those of the total fields, are in good agreement with their respective total fields. The coherent vorticity sheets and current density sheets are represented by 3.21% of the wavelet coefficients of vorticity, and by 3.16% of the wavelet coefficients of current density, respectively. Table 1 shows that the coherent parts retain almost all of the kinetic and magnetic energies, 93.2% of the kinetic enstrophy and 93.7% of the magnetic enstrophy.

In contrast, the incoherent vorticity and current density are structureless, as shown in Fig. 1 (right), respectively. Note that for the incoherent fields the values of the isosurfaces chosen for visualization are reduced by a factor of 3, as their fluctuations are much smaller than those of the total fields. These incoherent parts, reconstructed from the remaining large majority of the wavelet coefficients of vorticity and current density, retain little of the kinetic and magnetic energies: only 6.8% of the kinetic enstrophy, and 6.3% of the magnetic enstrophy (see Table 1).

3.1.2 Probability density functions

The probability density functions (PDFs) of the velocity and magnetic fields of the total, coherent and incoherent parts are plotted in Fig. 2 (left). The total and coherent velocity PDFs (two wide PDFs) coincide well. The incoherent velocity PDF is quasi-Gaussian with a strongly reduced variance compared to that of the total field. The same observations hold for the magnetic field.

In contrast, the vorticity and current density PDFs exhibit different behavior, as shown in Fig. 2 (right). Although the PDFs of the total and coherent fields of both vorticity and current density almost coincide, they show stretched exponential tails which show the intermittency that is due to the presence of coherent vorticity sheets and current density sheets. The PDFs of the incoherent fields have exponential shapes with reduced variances compared to those of the total fields. The skewness and flatness of the total, coherent and incoherent fields are listed in Table 2.

	coherent	incoherent	large scale	small scale
% of kinetic enstrophy	93.2	6.8	84.0	16.0
% of kinetic energy	99.8	0.1	99.8	0.2
% of magnetic enstrophy	93.7	6.3	83.0	17.0
% of magnetic energy	99.9	0.1	99.8	0.2

Table 1: Energies and enstrophies of the total, coherent, incoherent, large-scale and small-scale fields.

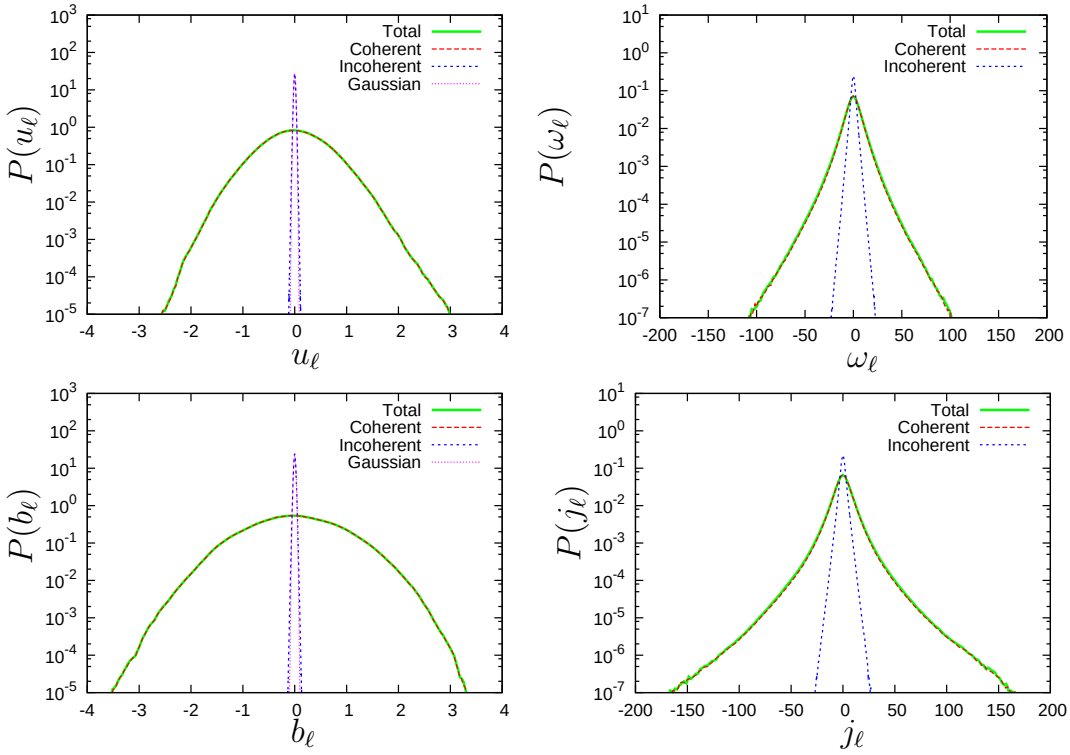

Figure 2: PDFs of the ℓth components of (top) the velocity and (bottom) the magnetic fields for the total, coherent and incoherent fields. (left) PDFs of the ℓth components of (top) the vorticity and (bottom) the current density fields for the total, coherent and incoherent fields. (right)

3.1.3 Energy spectra and energy fluxes

Figure 3 shows the kinetic and magnetic energy spectra, plotted versus the wavenumber normalized by Iroshnikov and Kraichnan (IK) microscale $\eta_{\rm IK}$, for the total, coherent and incoherent parts. The spectra are obtained by integrating energy in three-dimensional $\boldsymbol{k}$-space over spherical shells $k = |\boldsymbol{k}|$.

We observe that the spectra of the total fields exhibit an IK spectrum in the inertial subrange, i.e., $E^\zeta(k) \propto k^{-3/2}$ $(\zeta = u, b)$[12,13]. For the coherent contributions, the kinetic and magnetic energy spectra are identical with those of the total fields all along the inertial range, respectively. This implies that coherent vorticity sheets and current density sheets are responsible for the IK spectrum. Although both spectra of the coherent fields differ from the spectra of the total fields for $k\eta_{\rm IK} \gtrsim 0.5$, the coherent fields still provide significant contributions at scales smaller than $k\eta_{\rm IK} \simeq 0.5$. Concerning the incoherent fields, we observe that the scaling of the incoherent kinetic energy spectrum is close to k^2. This is also the case for the incoherent magnetic field. These k^2 spectra correspond to equipartitions of incoherent kinetic and magnetic energies between all wave vectors $\boldsymbol{k}$, respectively. The incoherent velocity and magnetic fields are therefore spatially decor-

Quantity	total	coherent	incoherent	large scale	small scale
Velocity skewness	0.055	0.055	0.000	0.055	−0.004
Velocity flatness	3.3	3.3	3.7	3.3	12.1
Magnetic field skewness	0.018	0.018	0.000	0.018	−0.002
Magnetic field flatness	3.0	3.0	3.7	3.0	16.8
Vorticity skewness	−0.050	−0.052	0.001	−0.029	−0.008
Vorticity flatness	8.1	8.4	5.8	5.5	16.3
Current density skewness	0.015	0.016	−0.001	0.009	0.001
Current density flatness	14.2	14.9	6.2	7.9	23.7

Table 2: Skewness and flatness for the total, coherent, incoherent, large-scale and small-scale fields.

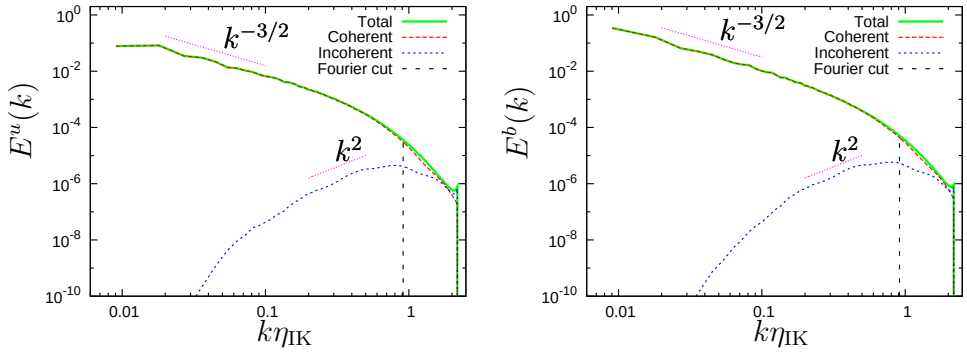

Figure 3: Kinetic (left) and magnetic (right) energy spectra of the total, coherent and incoherent fields.

related, which is consistent with the observation that incoherent vorticity and current density are structureless (see Fig. 1 (right)).

Studying the transfer of kinetic and magnetic energy in Fourier space enables us to check the contributions of the coherent and incoherent fields to the nonlinear dynamics. The energy fluxes for the kinetic and magnetic energy are defined by

$$\Pi_\alpha(k) = -\int_0^k T_\alpha(q)\mathrm{d}q, \tag{1}$$

$$\begin{aligned} T_\alpha(q) &= \frac{1}{2}\sum_{q-1/2\le q'<q+1/2} \left\{\mathcal{F}[\boldsymbol{z}_\alpha^-](\boldsymbol{q}')\cdot\mathcal{F}[\left(\boldsymbol{z}_\alpha^+\cdot\nabla\right)\boldsymbol{z}_\alpha^-](\boldsymbol{q}')\right. \\ &+ \left.\mathcal{F}[\boldsymbol{z}_\alpha^+](\boldsymbol{q}')\cdot\mathcal{F}[\left(\boldsymbol{z}_\alpha^-\cdot\nabla\right)\boldsymbol{z}_\alpha^+](\boldsymbol{q}')\right\}, \quad \alpha = \mathrm{c},\mathrm{t} \end{aligned} \tag{2}$$

where $q = |\boldsymbol{q}|$, $\boldsymbol{z}_\mathrm{c}^\pm = \boldsymbol{u}_\mathrm{c} \pm \boldsymbol{b}_\mathrm{c}$ and $\boldsymbol{z}_\mathrm{t}^\pm = \boldsymbol{u} \pm \boldsymbol{b}$.

Figure 4 shows the energy fluxes for the coherent fields, normalized by the energy dissipation rate $\langle\epsilon\rangle$ versus $k\eta_{\mathrm{IK}}$, together with the total energy flux. We find that the energy flux for the coherent fields coincides with that for the total fields all along the inertial range. In the dissipative range, the coherent flux still dominates, though it begins to depart from the total flux.

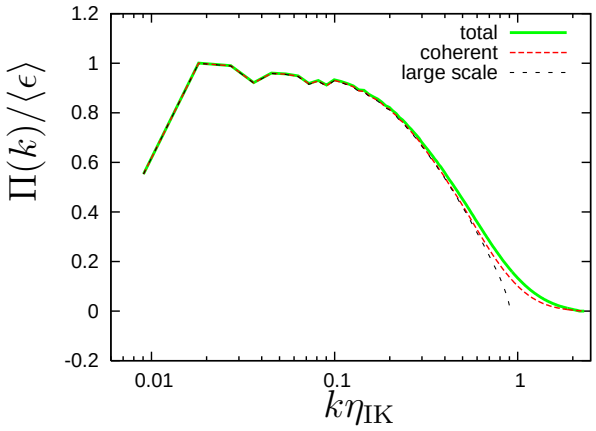

Figure 4: Energy fluxes $\Pi(k)$ for the total, coherent and large-scale fields.

3.2 Results obtained by LFF method

3.2.1 Visualization

Figure 5 (left) shows that the large-scale vorticity (top) and current density (bottom) structures, both represented by 3.26% of the Fourier coefficients, retain less vorticity and current density sheets than the coherent vorticity and current density fields (see Fig. 1). Table 1 shows that the large-scale fields retain almost all of the kinetic and magnetic energies, but have less kinetic and magnetic enstrophies than the coherent fields.

Figure 5 (right) illustrates that the small-scale vorticity and current density fields exhibit organized structures, similar to those present in the DNS field. This is in contrast with the incoherent fields, which contain no vorticity and current density sheets as shown in Fig. 1 (right). Table 1 shows that the small-scale fields have more kinetic and magnetic enstrophies than the incoherent fields.

3.2.2 Probability density functions

Figure 6 (left) shows that the PDFs of the large-scale velocity and magnetic fields are in good agreement with those of the total velocity and magnetic fields, respectively. This is the case for the coherent fields, which preserve the PDFs of the total velocity and magnetic fields. The PDFs of the small-scale velocity and magnetic fields exhibit a stretched exponential behavior, though the incoherent velocity and magnetic fields exhibit a quasi-Gaussian distribution (see Fig. 2).

Figure 6 (right) reveals that the PDFs of the large-scale vorticity and current density, $\boldsymbol{\omega}_{\mathrm{L}}$ and $\boldsymbol{j}_{\mathrm{L}}$, do not preserve those of the total fields. The small-scale vorticity and current density has about the same range of variation as $\boldsymbol{\omega}_{\mathrm{L}}$ and $\boldsymbol{j}_{\mathrm{L}}$, respectively. These results about the PDFs of $\boldsymbol{\omega}_{\mathrm{L}}$ and $\boldsymbol{j}_{\mathrm{L}}$ are in contrast with those obtained by the CVCE method. As mentioned in subsection 3.1.2, the PDFs of the coherent vorticity and current density

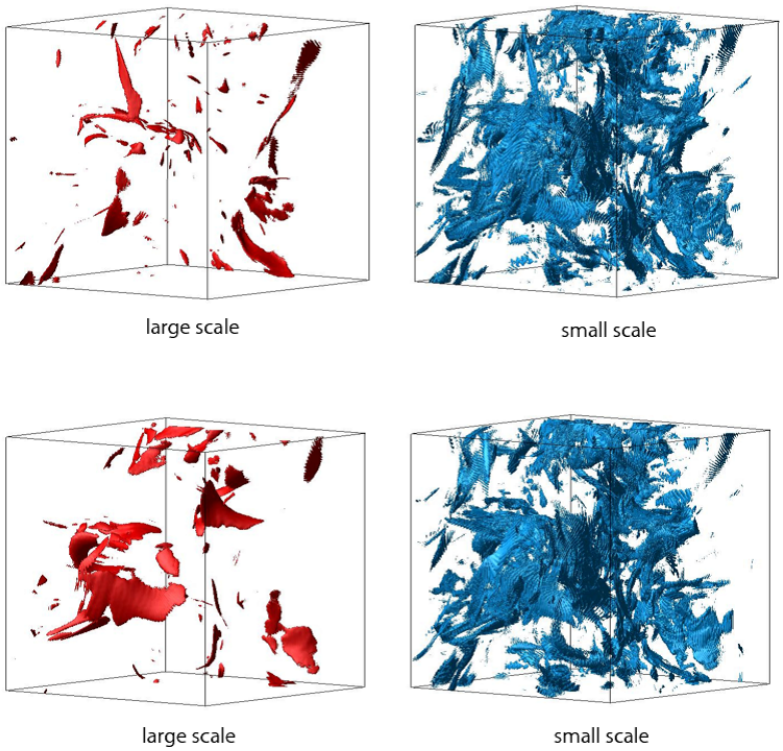

Figure 5: Isosurfaces of $|\boldsymbol{\omega}|$ (top) and $|\boldsymbol{j}|$ (bottom) of the large-scale (left), and small-scale contributions (right). The values of the isosurfaces are the same as those for the corresponding coherent and incoherent fields. Subcubes of size 256^3 are visualized.

fields well preserve those of the total fields. The spatial variations of the incoherent vorticity and current density fields are much smaller than those of the coherent vorticity and current density fields.

3.2.3 Energy spectra and energy fluxes

We have denoted the cutoff wavenumber k_c separating the large- and small-scale contributions by vertical dashed lines in Fig. 3. The energy spectra of the large-scale velocity and magnetic fields are identical with those of the total fields for $k < k_c$, and the energy spectra of the small-scale velocity and magnetic fields are the same as those for $k \geq k_c$.

The energy fluxes for the large-scale fields are obtained by the use of the equation (1) with replacement of $\boldsymbol{z}_\alpha^\pm$ by $\boldsymbol{z}_L^\pm = \boldsymbol{u}_L \pm \boldsymbol{b}_L$. Figure 4 shows that the large-scale fields preserve the nonlinear dynamics of the DNS field in the inertial range, but not near the cutoff wavenumber.

4 CONCLUSIONS

We have introduced the coherent vorticity and current density extraction (CVCE) method for extracting coherent structures from MHD turbulent fields[9] and compared the

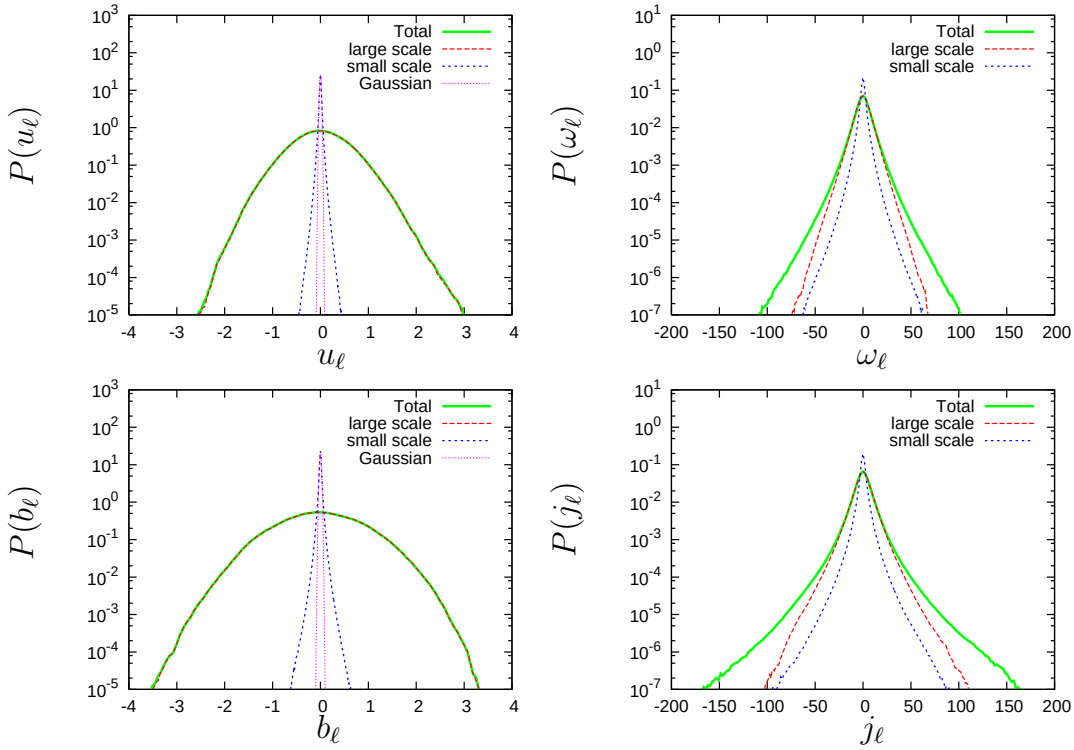

Figure 6: PDFs of the ℓth components of (top) the velocity and (bottom) the magnetic fields for the total, large-scale and small-scale fields. (left) PDFs of the ℓth components of (top) the vorticity and (bottom) the current density fields for the total, large-scale and small-scale fields. (right)

method with the linear Fourier filtering (LFF) method. The CVCE method is based on the orthogonal wavelet decomposition. Thresholding the wavelet coefficients allows us to split each of the fields into two contributions: a coherent and organized component, and an incoherent and random component. The LFF method is based on the Fourier decomposition, which decomposes the fields into large- and small-scale contributions. Both methods have been applied to the DNS data of incompressible MHD turbulence without mean magnetic field in a 2π periodic box, computed at resolution $N = 512^3$ with the Taylor microscale Reynolds number $R_\lambda^M = 157$.

The coherent structures extracted by the CVCE method, reconstructed from few wavelet coefficients, preserve the coherent vorticity sheets and current density sheets present in the DNS field. The coherent fields contain most of the kinetic and magnetic energies and enstrophies of the total fields. The PDFs of the total and coherent vorticity and current density have stretched exponential tails and coincide almost perfectly. The coherent kinetic and magnetic energy spectra coincide with the spectra of the total fields all along the inertial range, and they differ only in the dissipative range. Studying the flux of the kinetic and magnetic energy confirms that the nonlinear dynamics is fully captured by the coherent fields.

The large-scale fields, represented by almost the same number of degrees of freedom as that of the coherent fields, do not well preserve vorticity sheets and current density sheets present in the DNS field. The large-scale fields contain most of the kinetic and magnetic energies of the DNS field. However, they retain less kinetic and magnetic enstrophies than the coherent fields. The PDFs of the large-scale vorticity and current density do not preserve those of the total vorticity and current density fields. The flux of the kinetic and magnetic energies of the DNS field is retained well by the large-scale fields in the inertial range, but not near the cutoff wavenumber.

In conclusion, the wavelet representation is more suitable for extracting the coherent structures and preserving the statistics of the total fields than the Fourier representation. The above findings motivate the development of Coherent Vorticity sheet and Current density sheet Simulation method (CVCS), which is a generalization of the Coherent Vortex Simulation method (CVS). CVS is based on the deterministic computation of the coherent flow evolution using an adaptive wavelet basis and modeling the influence of the incoherent background flow, which was proposed for hydrodynamic turbulence.[14] Applications of CVS to two-dimensional flows and to three-dimensional turbulent mixing layers can be found in Refs. 15−17. Thus, CVCS is promising and should be pursued in future studies.

ACKNOWLEDGEMENTS

The computations were carried out on the HPC2500 and FX systems at the Information Technology Center of Nagoya University. This work was supported by a Grant-in-Aid for Young Scientists (B) 20760055 from the Ministry of Education, Culture, Sports, Science and Technology of Japan. MF and KS acknowledge financial support from the Agence Nationale de la Recherche, project "M2TFP" and from the Association CEA-Euratom.

REFERENCES

1. M. Farge, Wavelet transforms and their applications to turbulence, *Annu. Rev. Fluid Mech.*, **24**, 395–457 (1992).

2. K. Schneider, and O. Vasilyev, Wavelet Methods in Computational Fluid Dynamics, *Annu. Rev. Fluid Mech.*, **42**, 473–503 (2010).

3. M. Farge, K. Schneider and N. Kevlahan, Non-Gaussianity and coherent vortex simulation for two-dimensional turbulence using an adaptive orthonormal wavelet basis, *Phys. Fluids*, **11**, 2187–2201 (1999).

4. M. Farge, G. Pellegrino and K. Schneider, Coherent vortex extraction in 3D turbulent flows using orthogonal wavelets, *Phys. Rev. Lett.*, **87**, 054501 (2001).

5. M. Farge, K. Schneider, G. Pellegrino, A. A. Wray and R. S. Rogallo, Coherent vortex extraction in three-dimensional homogeneous turbulence: comparison between CVS-wavelet and POD-Fourier decompositions, *Phys. Fluids*, **15**, 2886–2896 (2003).

6. S. Mallat, A wavelet tour of signal processing, *Academic Press*, (1998).

7. D. Donoho and I. Johnstone, Ideal spatial adaptation via wavelet shrinkage, *Biometrika*, **81**, 425–455 (1994).

8. N. Okamoto, K. Yoshimatsu, K. Schneider, M. Farge, and Y. Kaneda, Coherent vortices in high resolution direct numerical simulation of homogeneous isotropic turbulence: A wavelet viewpoint, *Phys. Fluids*, **19**, 115109 (2007).

9. K. Yoshimatsu, Y. Kondo, K. Schneider, N. Okamoto, H. Hagiwara, M. Farge, and Y. Kaneda, Wavelet-based coherent vorticity sheet and current sheet extraction from three-dimensional homogeneous magnetohydrodynamic turbulence, *Phys. Plasmas*, **16**, 082306 (2009).

10. H. Politano, A. Pouquet and P. L. Sulem, Current and vorticity dynamics in three-dimensional magnetohydrodynamic turbulence, *Phys. Plasmas*, **2**, 2931 (1995).

11. P. D. Mininni, A. G. Pouquet and D. C. Montgomery, Small-Scale Structures in Three-Dimensional Magnetohydrodynamic Turbulence, *Phys. Rev. Lett.*, **97**, 244503 (2006).

12. P. S. Iroshnikov, Turbulence of a conducting fluid in a strong magnetic field, *Sov. Astron.*, **7**, 566–571 (1963).

13. R. H. Kraichnan, Inertial-range spectrum of hydrodynamics turbulence, *Phys. Fluids*, **8**, 1385–1387 (1965).

14. M. Farge and K. Schneider, Coherent vortex simulation (CVS), a semi-deterministic turbulence model using wavelets, *Flow Turbul. and Combust.*, **66**, 393–426 (2001).

15. K. Schneider, M. Farge, A. Azzalini and J. Ziuber, Coherent vortex extraction and simulation of 2d isotropic turbulence, *J. Turbul.*, **7**, 44 (2006).

16. K. Schneider, M. Farge, G. Pellegrino, and M. Rogers, Coherent vortex simulation of 3d turbulent mixing layers using orthogonal wavelets, *J. Fluid Mech.*, **534**, 39–66 (2005).

17. O. Roussel, and K. Schneider , Coherent Vortex Simulation of weakly compressible turbulent mixing layers using adaptive multiresolution methods, *J. Comput. Phys.*, 229, 2267–2286 (2010).